Molecular Self-Assembly of Functionalized Fullerenes on a Metal Surface

Bogdan Diaconescu,[1,*] Teng Yang,[2] Savas Berber,[2,†] Mikael Jazdzyk,[3] Glen P. Miller,[3] David Tománek,[2] and Karsten Pohl[1]

[1]*Department of Physics and Materials Science Program, University of New Hampshire, Durham, New Hampshire 03824, USA*
[2]*Physics and Astronomy Department, Michigan State University, East Lansing, Michigan 48824-2320, USA*
[3]*Department of Chemistry and Materials Science Program, University of New Hampshire, Durham, New Hampshire 03824, USA*

(Received 23 July 2008; published 5 February 2009)

We present a combined experimental and theoretical study of the self-assembly of C_{60} molecules functionalized with long alkane chains on the (111) surface of silver. We find that the conformation of the functionalized C_{60} changes upon adsorption on Ag(111) and that the unit cell size in the self-assembled monolayer is determined by the interactions between the functional groups. We show that C_{60} molecules can be assembled in ordered 2D arrays with intermolecular distances much larger than those in compact C_{60} layers, and propose a novel way to control the surface pattern by appropriate chemical functionalization.

DOI: 10.1103/PhysRevLett.102.056102 PACS numbers: 68.43.Hn, 68.35.bm, 68.37.Ef, 68.43.Bc

Ordered arrays of molecules or nanoparticles such as C_{60} fullerenes have a great number of practical applications, ranging from sensors and biological interfaces [1] to organic electronics [2], photovoltaics, and novel computational methods such as quantum dot cellular automata and, with endohedral fullerenes, a spin-based quantum computer [3,4]. Generally speaking, self-assembled monolayers (SAM) of molecules form as a result of a delicate balance between competing molecule-substrate and intermolecular interactions [5]. Therefore, to control such self-assembly processes and grow molecular arrays of designed geometries, it is mandatory to understand how this balance reflects onto the SAM's final structure [6,7].

Here we describe a novel way of controlling the self-assembly process and designing the structure of SAMs via chemical functionalization of the C_{60} cages. Self-organization of C_{60} cages in ordered arrays at desired non-close-packed distances can be achieved by controlling the hierarchy of interactions within the SAM, in accordance with *ab initio* total energy calculations. Our scanning tunneling microscopy (STM) images show that C_{60} cages functionalized with two long alkane tails [Fig. 1(a)], once grown onto the close-packed surface of Ag, self-assemble into parallel zigzag rows [Fig. 1(b)], the separation of which is determined by the length of the tails.

We chose to synthesize this functionalized fullerene [8] in order to exploit several intermolecular interactions during the assembly on Ag(111). These interactions include fullerene-fullerene π-π stacking interactions [9,10], alkyl-alkyl interchain interactions and substrate-molecule interactions. The peculiar dimerization pattern in the zigzag rows can be traced back to a conformational change of the functionalized C_{60} molecule (F-C_{60}) upon adsorption. The conformational change and the self-assembled molecular pattern are a consequence of a hierarchy of interactions within the SAM, which can be explained by *ab initio* density functional theory (DFT) calculations.

We studied the self-assembled monolayers on an atomically flat thin film of silver used as substrate. The Ag film, with a thickness of two atomic Ag layers or more, was grown on the (0001) surface of a single crystal ruthenium sample by physical vapor deposition under ultrahigh vacuum (UHV) conditions and has a (111) orientation. Functionalized C_{60} molecules [8], depicted in Fig. 1(a), have then been deposited *in situ* on freshly prepared Ag films by low temperature sublimation at about 520 K. Following the F-C_{60} deposition, annealing of the sample at 420 to 470 K was performed for a few minutes in order to

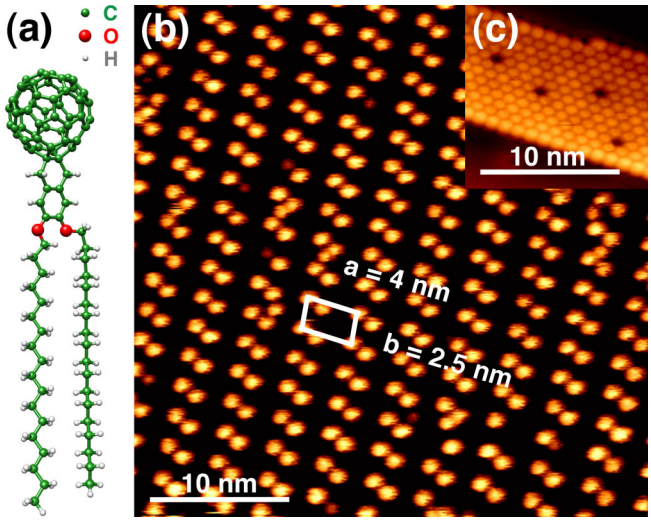

FIG. 1 (color online). Self-assembled monolayer of F-C_{60} on Ag(111). (a) Ground state structure of an isolated F-C_{60} molecule containing 2.2 nm long alkyl chains with 18 C atoms each, bonded covalently to a C_{60} cage. (b) STM constant current image of F-C_{60} SAM (295 K, −1 V sample bias, 0.4 nA) also showing the geometry of the unit cell of the molecular structure. (c) Island of pristine C_{60} on Ag(111) imaged in identical conditions (295 K, −1 V, 0.4 nA).

increase the size of the ordered SAM domains. The sample preparation and analysis took place in a home-built variable temperature STM operating in UHV at a base pressure of 1×10^{-10} torr [11]. The STM data presented here were acquired at room temperature (295 K).

Figure 1(b) shows a constant current STM image of an ordered domain of F-C_{60} molecules. The molecular 2D superstructure forms a 4 nm $\times$ 2.5 nm oblique unit cell with a sharp angle of about 80°, in stark contrast to the triangular close-packed arrangement of pristine C_{60} grown in UHV conditions on an identically prepared Ag(111) surface [Fig. 1(c)]. The bright spherical symmetrical features in the F-C_{60} SAM image, shown in Fig. 1(b), are the fingerprint of the fullerene cages, as tested against pure fullerenes imaged in identical tunneling conditions [Fig. 1(c)]. The darker areas between those features correspond to the regions where the alkane chains lie down on the Ag(111) surface. The measured distances between the first and second nearest neighbor fullerene cages are about 1.6 nm and 2.0 nm. These distances are larger than the C_{60}-C_{60} close-packed interaction distance of 1.0 nm [Fig. 1(c)] [12]. It is somewhat surprising that the functionalized fullerenes do not assemble in such a manner as to maximize fullerene-fullerene π-π stacking interactions given that fullerenes are known to assemble on Ag into hexagonal close-packed 2D island domains [12] as seen in Fig. 1(c). The implication is that fullerene-fullerene π-π stacking interactions are weaker than other prevailing interactions that drive the patterning during assembly.

Since experimental data have low contrast associated with individual F-C_{60} alkane tails (presumably because of the high corrugation of the SAM), a detailed analysis of the F-C_{60} STM signature is needed. Interpretation of the STM images is often counterintuitive since the tunneling current is correlated with wave functions near the Fermi level rather than atomic positions. This is best illustrated by plotting the charge distribution associated with the highest occupied molecular orbital (HOMO) and the lowest unoccupied molecular orbital (LUMO). These orbitals, based on DFT calculations described below, are shown in Figs. 2(a) and 2(b). When adsorbed on the Ag(111) surface, the nature of states imaged by STM changes dramatically due to the hybridization between the electronic states of the substrate and the molecular orbitals of F-C_{60}. Calculated contours of constant tunneling current for F-C_{60}, shown in Fig. 2(c), agree well with the experimentally observed corrugation of 0.65 nm of the SAM, shown in Fig. 2(d).

Significantly more crystallographic information about the F-C_{60} SAM structure can be obtained from larger scale STM images. Figure 3 shows all the observed orientations of the F-C_{60} ordered domains. The image also contains two Ag steps oriented along a compact direction of the (111) surface. We see that the F-C_{60} SAM domains are oriented in six distinct directions, identified by lines coinciding with the direction of the short side of the unit cell in Fig. 1(b). These domains can be subdivided into two groups containing three distinct directions, separated by 60°. These two groups of sixfold symmetries suggest a preferential orientation of the F-C_{60} molecules with the alkane tails aligned along a high symmetry direction on Ag(111), such as the most or the least compact direction of the substrate. Any domain of one group is related to a domain of the other group by a reflection operation on a compact direction of Ag(111), under which the Ag(111) surface is invariant. This finding suggests that the F-C_{60} molecule possesses

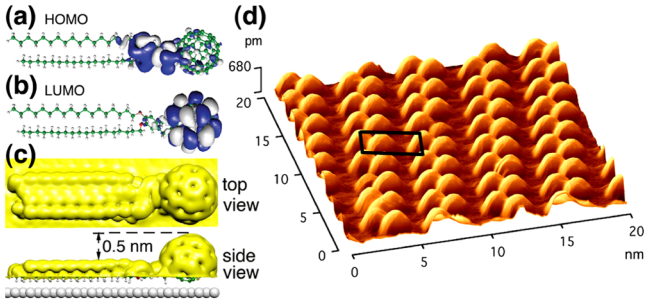

FIG. 2 (color online). F-C_{60} STM signature. Wave functions of (a) the HOMO and (b) the LUMO of the free F-C_{60} molecule, superposed with the atomic structure. (c) Calculated contours of constant local density of states for an F-C_{60} molecule on Ag(111) representing constant current STM images under experimental conditions. (d) 3D representation of the STM data showing the corrugation of the F-C_{60} SAM (295 K, -1 V, 0.4 nA). The lateral size of the fullerene is a consequence of the tip shape convolution.

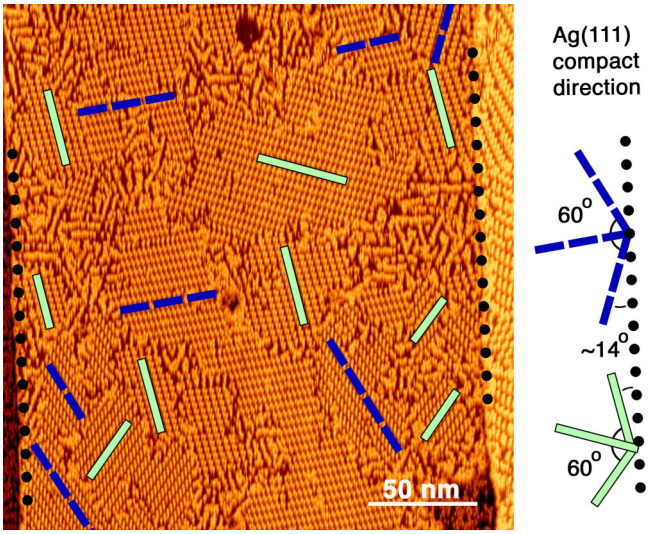

FIG. 3 (color online). Large scale STM image of F-C_{60} SAM on 2 ML Ag/Ru(0001). The terrace edges of the Ag(111) substrate, corresponding to one of its compact directions, are marked by the dotted lines. The F-C_{60} self-assemble in domains with six different orientations, shown schematically in the diagram. We distinguish two domain groups, characterized by the solid bright green and dashed dark blue lines. Each group contains three types of domains with distinct orientations, separated by 60°. The sharpest angle between any domain direction and a Ag(111) compact direction is 14°.

two mirror image configurations once adsorbed onto the metal surface.

To obtain fundamental insight into the origin of the SAM pattern of F-C_{60} molecules on Ag(111), we determined the optimum geometry, binding energy and electronic structure of these systems at $T = 0$ via *ab initio* DFT calculations [13]. We used the local density approximation and the Perdew-Zunger [14] parametrization of the exchange-correlation functional. Most total energy calculations were performed using the QUANTUM-ESPRESSO code [15] with ultrasoft pseudopotentials [16] and employed a plane-wave basis with a 25 Ry kinetic energy cutoff. We calculated the charge density in real space on a mesh equivalent to a 200 Ry cutoff energy, and used Ag pseudopotentials containing 4*d* semicore orbitals. We sampled the Ag(111) Brillouin zone by a $32 \times 32 \times 1$ *k*-point mesh and adjusted the mesh density for F-C_{60}/Ag(111) systems with larger unit cells. The vacuum region between 2D slabs was taken larger than 1 nm to minimize the interlayer interaction.

Selected structure optimizations were performed using the SIESTA code [17] with a double-ζ polarized basis localized at the atomic sites. The valence electrons were described by norm-conserving Troullier-Martins pseudopotentials [18] in the Kleinman-Bylander factorized form [19]. We used the counterpoise method [20] to avoid basis-set superposition errors (BSSE) introduced by the localized basis and found the BSSE corrected local basis results in good agreement with our plane-wave results. We used 1–4-layer slab representations of Ag(111) and periodic boundary conditions. In the superlattice geometry, the slabs were separated by 2 nm in the normal direction and represented by orthorhombic unit cells containing 2–8 silver atoms. The supercells were sampled by a $32 \times 32 \times 1$ *k*-point mesh. The self-consistent charge density was obtained using a real-space grid with a mesh cutoff energy of 250 Ry, achieving a total energy convergence better than 0.05 meV/atom.

We next discuss separately the mutual interactions between the substrate, alkane chains, and fullerenes. The final structure of the F-C_{60}/Ag(111) monolayer will be determined by the hierarchy of interactions between these constituents.

Since the functional tail of F-C_{60} contains alkane chains, we performed total energy calculations of infinite polyethylene chains adsorbed on Ag(111) along various directions. As seen in Fig. 1(a), the zigzag carbon backbone of an alkane chain lies in a plane that may be used to identify the chain orientation. We found the adsorption energy of 0.22 eV along the most compact direction, with the carbon backbone parallel to the surface, and with the C atoms in the trough, to be the most stable. All adsorption energies are normalized per C_2H_4 segment. The energy cost to displace the polymer across the surface, while maintaining its direction and orientation, is less than 0.02 eV per C_2H_4. Keeping the carbon backbone parallel to the surface, but changing the orientation from the most compact to the least compact direction, occurs at an energy cost of 0.01 eV. Displacing the chain across the surface in this orientation occurs at an even lower energy cost of less than 0.001 eV. Comparing polymers aligned along the same direction on the Ag(111) surface, we found that polymers with the backbone normal to the surface are less bound by 0.05 eV than polymers with the backbone parallel to the surface.

Although the alkyl chains of the free F-C_{60} molecules have many conformational degrees of freedom, the optimized geometry representing the global minimum [Fig. 1(a)] places the C backbones of the adjacent alkyl chains normal to each other. Our calculations indicate that the alkane tail will gain 0.05 eV per C_2H_4 segment, when both alkane tails adsorb with the C backbone plane parallel to the surface. In the free molecule, rotating one of the chains around the virtual hinge of a C-O bond to make the backbones coplanar is associated with a moderate energy gain of about 0.2 eV. However, during this rotation, the chains assume the *V* configuration [Fig. 4(b)], therefore eliminating the attractive interaction between the neighboring chains and as such necessitating a net energy investment of 0.42 eV for the entire F-C_{60} molecule. We find the opening angle between the alkane chains in the optimized structure to be 30°–40°, which would be expected for rigid bonds and bond angles. The improved interaction between the chains and the substrate results in a net energy gain of 0.48 eV for the entire molecule, suggesting that adsorbed F-C_{60} molecules undergo a conformational change from

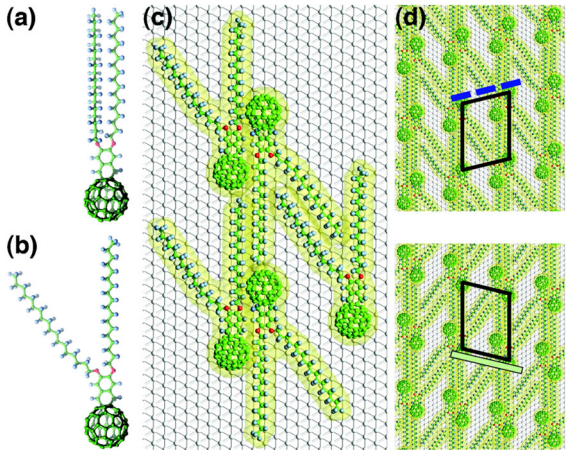

FIG. 4 (color online). Ground state configurations of a free and an adsorbed F-C_{60} molecule: (a) *I* shape configuration and (b) *V* shape configuration. (c) Detail of the F-C_{60} assembling in the optimum geometry. (d) Adsorbtion geometries of the F-C_{60} SAM resulting from the proposed model. Besides the backbone of the F-C_{60} molecules, we also depict the envelope associated with the van der Waals radii of the atoms. The primitive unit cell depicted by the black lines, containing two F-C_{60} molecules, agrees with the unit cell shown in Fig. 1(b). The dashed dark blue and solid bright green lines, aligned with a unit cell side, correspond to the domain orientations in Fig. 3.

the *I* shape, representative for the free molecule [Fig. 4(a)], to the *V* shape [Fig. 4(b)] upon adsorption on Ag(111).

The C_{60} adsorption energy on Ag(111) is sensitive to substrate relaxation and increases from 0.84 eV on a monolayer to 1.22 V on a 4-layer slab, with energy differences below 0.03 eV depending on the orientation of the C_{60}, in qualitative agreement with Ref. [21]. In equilibrium, depending on orientation, the center of the C_{60} cage lies about 0.60–0.65 nm above the Ag(111) surface.

Addressing separately the intermolecular interactions between various constituents, we found that adjacent C_{60} cages bind to each other with 0.15 eV at the equilibrium distance of 1 nm. Also, long chain alkanes bind with 0.27 eV to a fullerene cage, but interact very weakly with the phenyl rings connecting the C_{60} to the alkane tails. Finally, two infinite polyethylene chains, both with their C backbones parallel to the Ag(111) surface, experience an attractive interaction of 0.06 eV per C_2H_4 segment at their equilibrium separation of 0.43 nm [13] and a separation from the substrate of 0.32 nm.

The ground state structure of the F-C_{60} SAM on Ag(111) is illustrated in Figs. 4(c) and 4(d). As discussed above, the F-C_{60} undergoes a conformational change from the *I* shape, representative for the free molecule [Fig. 4(a)], to the *V* shape [Fig. 4(b)] upon chemisorption. The structure in Fig. 4(c) furthermore maximizes the interaction between the alkane chains and the C_{60} ends of the F-C_{60} molecules. The optimum angle between the chains of the F-C_{60} molecules, which is about 30° in Fig. 4(c), may be modified to some degree in order to maximize the interchain interaction. When optimizing the SAM geometry, we also must consider the fact that the alkane tails lie much closer to the substrate than the fullerene cages, suggesting an apparent overlap between the two when viewed from top as probed by the STM tip. The orientation of the SAM on Ag(111) is likely given by the preference of at least one of the alkane tails in each F-C_{60} molecule to align along the most compact direction, as shown in Fig. 4(c). Moreover, the model generates all the possible orientations of the SAM with respect to the Ag(111) surface [Fig. 4(d)], observed as simultaneously occurring domains in Fig. 3. Thus, the self-assembly process selects molecules of given mirror configuration once adsorbed on the surface in individual domains. The overall calculated adsorption pattern therefore explains the observed unit cell size and shape, including the distances between neighboring C_{60} ends of the F-C_{60} molecules. The alkane chain conformations are the reason for the formation of the intriguing asymmetric zigzag pattern observed here.

Given the fundamental nature of our calculations and the good agreement with the experimental data, we can use our insight to predict the behavior of related systems on other substrates. The pattern depicted in Figs. 4(c) and 4(d) should not only occur on Ag(111), but on any substrate where the energetic preference for the alkane chains to adsorb with their backbones parallel rather than normal to the substrate is sufficiently large to initiate the *V*-shape configuration of Fig. 4(b). We also expect patterns with oblique, but larger unit cells, if the chain length in F-C_{60} increases. Other monolayer patterns could be obtained by changing the relative length of the alkyl chains attached to the C_{60} molecule.

This work was supported by the Nanoscale Science and Engineering Center for High-Rate Nanomanufacturing (NSF NSEC-425826). Computational resources have been provided by the Michigan State University High Performance Computing Center. B. D. and K. P. also acknowledge support from NSF DMR-0134933, and T. Y., S. B., and D. T. from NSF-NIRT ECS-0506309.

*bogdan@einstein.unh.edu

†Permanent address: Physics Department, Gebze Institute of Technology, 41400 Gebze, Kocaeli, Turkey.

[1] D. Bonifazi, O. Euger, and F. Diederich, Chem. Soc. Rev. **36**, 390 (2007).
[2] C. Joachim, J. K. Gimzewski, and A. Aviram, Nature (London) **408**, 541 (2000).
[3] S. Lloyd, Science **261**, 1569 (1993).
[4] W. Harneit, Phys. Rev. A **65**, 032322 (2002).
[5] J. V. Barth, G. Constantini, and K. Kern, Nature (London) **437**, 671 (2005).
[6] F. Rosei, M. Schunack, Y. Naitoh, P. Jiang, A. Gourdon, E. Laegsgaard, I. Stensgaard, C. Joachim, and F. Besenbacher, Prog. Surf. Sci. **71**, 95 (2003).
[7] B. Xu, C. Tao, W. G. Cullen, J. E. Reutt-Robey, and E. D. Williams, Nano Lett. **5**, 2207 (2005).
[8] *Ortho*-catechol was alkylated using 1-iodooctadecane and then bromomethylated to produce 1,2-dioctadecyloxy-4,5-dibromomethylbenzene. Reaction with KI/18-crown-6 generates the corresponding quinodimethane which undergoes a [4 + 2] cycloaddition to produce the functionalized fullerene.
[9] G. P. Miller and J. Mack, Org. Lett. **2**, 3979 (2000).
[10] G. P. Miller and J. B. Briggs, Org. Lett. **5**, 4203 (2003).
[11] B. Diaconescu, G. Nenchev, J. de la Figuera, and K. Pohl, Rev. Sci. Instrum. **78**, 103701 (2007).
[12] E. I. Altman and R. J. Colton, Phys. Rev. B **48**, 18 244 (1993).
[13] T. Yang, S. Berber, J. F. Liu, G. P. Miller, and D. Tomanek, J. Chem. Phys. **128**, 124709 (2008).
[14] J. P. Perdew and A. Zunger, Phys. Rev. B **23**, 5048 (1981).
[15] S. Baroni *et al.*, http://www.pwscf.org/.
[16] D. Vanderbilt, Phys. Rev. B **41**, 7892 (1990).
[17] J. M. Soler, E. Artacho, J. D. Gale, A. García, J. Junquera, P. Ordejón, and D. Sánchez-Portal, J. Phys. Condens. Matter **14**, 2745 (2002).
[18] N. Troullier and J. L. Martins, Phys. Rev. B **43**, 1993 (1991).
[19] L. Kleinman and D. M. Bylander, Phys. Rev. Lett. **48**, 1425 (1982).
[20] S. F. Boys and F. Bernardi, Mol. Phys. **19**, 553 (1970).
[21] L.-L. Wang and H.-P. Cheng, Phys. Rev. B **69**, 165417 (2004).